Colloids and Surfaces B: Biointerfaces 183 (2019) 110451

Contents lists available at ScienceDirect

Colloids and Surfaces B: Biointerfaces

journal homepage: www.elsevier.com/locate/colsurfb

Impedimetric ultrasensitive detection of chloramphenicol based on aptamer MIP using a glassy carbon electrode modified by 3-ampy-RGO and silver nanoparticle

Mahmoud Roushani[a,*], Zeinab Rahmati[a], S. Jafar Hoseini[b], Roghayeh Hashemi Fath[c]

[a] Department of Chemistry, Ilam University, Ilam, Iran
[b] Professor Rashidi Laboratory of Organometallic Chemistry, Department of Chemistry, College of Sciences, Shiraz University, Shiraz, 7194684795, Iran
[c] Department of Chemistry, Faculty of Sciences, Yasouj University, Yasouj 7591874831, Iran

ARTICLE INFO

Keywords:
Aptamer
Molecular imprinting polymer
Chloramphenicol
Impedimetric detection
Electropolymerization

ABSTRACT

In this research work, a biosensor with a dual recognition system was fabricated and founded on a combination of aptasensing and the molecular imprinting union of the chloramphenicol (CAP) selective detection. CAP, is an antibiotic, was applied in veterinary and human in order to treat gram-positive and gram-negative infections. It is worth mentioning that CAP residue brings about earnest side effects on human health. According to this, in this sensing system, 3-aminomethyl pyridine functionalized graphene oxide (GO) (3-ampy-RGO) has been coated on the surface of GCE. Afterwards, the silver nanoparticle (AgNPs) was coated on the 3-ampy-RGO/GCE and, then, the CAP complex-amino-aptamer (NH_2-Apt[CAP]) was attached to the AgNP/3-ampy-RGO/GCE using a kind of bonding formation of Ag-N. In this sense, it is worth noting that the resorcinol electropolymerization around the complex of aptamer/CAP would confine the complex and, then, retain the aptamer. Following the CAP removal, the MIP cavity, as it was supposed, synergistically acted with that of the embedded aptamer in order to construct a nanohybrid receptor. Interestingly, the double exact property of the molecular imprinting polymers and aptamers led to the superb sensing properties. In the mentioned system it was illustrated that the linear range was from 1.0 pM to 1.0 nM with the detection limit of 0.3 pM; consequently, as observed, it was better than or as good as other similar assays. Moreover, the mentioned system whose activity was observed in the various interferences presence showed great selectivity in detected the CAP. Finally, the designed sensor exhibited outstanding results when applied to detect CAP in milk samples.

1. Introduction

Chloramphenicol (CAP) which has been regarded as a broad spectrum antibiotic can be applied in veterinary and human to cure Gram-positive and Gram-negative infections [1]. In this respect, CAP can have significant side effects in humans; i.e. aplastic anemia, leukemia, and gray-syndrome which were banned by the European Union to be used in both human and food producing animals [2–4]. But, in opposition to these legal bans, CAP can still be found in some animal-derived foods because of its low cost, easy access, its significant effects on the infection control, and also its effects on the production increase [5]. Thus, there exists a great demand for developing sensitive methods for the CAP residue detection in serum and foods derived from animal. In this way, some specific analytical approaches have been developed in order to determine CAP i. e. liquid chromatography mass spectrometry (LC–MS) [6,7], high performance liquid chromatography (HPLC) [8,9], capillary electrophoresis (CE) [1], colorimetry [10,11], ion chromatographiy [12], gas chromatography [13], molecularly imprinted polymers [14–16], chemiluminescence [17], photoelectrochemical aptasensor [18,19], and fluorescence [20,21]. Moreover, some other analytical approaches which have attempted to apply aptamers have been accurately launched for the CAP detection [5,22–24].

Molecular imprinting process was applied in which polymerizing functional monomers were used around a template in order to form the polymer-binding cavities which present chemical and steric selectivity for the target and template molecular kinds [25]. In theory, one can prepare the imprinted polymers for any interest analyte. It can be concluded that around 10,000 biological structures and molecules have been successfully imprinted in relation to the templates as multiple as proteins, inorganic ions, viruses, drugs, nucleic acids, and even cells [26,27]. MIPs, as being compared to the biological receptors, e.g. antibodies and aptamers, possess numerous advantages such as high

* Corresponding author.
E-mail address: m.roushani@ilam.ac.ir (M. Roushani).

https://doi.org/10.1016/j.colsurfb.2019.110451
Received 5 March 2019; Received in revised form 8 July 2019; Accepted 20 August 2019
Available online 21 August 2019

selectivity, physically and mechanically stability, low cost of preparation, and resistance. Nevertheless, MIPs would poor-binding attachment [26]. Aptamers which can be considered as oligonucleotides with high-binding affinity possess specificity for target molecules. Thus, Aptamers have been applied in order prepare a reliable ground for molecular diagnostics [5]. Hence, when biological ligands are combined in MIPs, it would provide selective binding to target molecules [28]. The hybrid-MIP system has been very helpful for macromolecular imprinting in order to generate hybrid-synthetic receptors which show higher binding characteristics [29].

This study aims at developing a hybrid-MIP receptor to be used in an electrochemical sensor which targets the CAP antibiotic quantitative analysis and ultrasensitive detection. Aptamers, as bio receptors, have been applied in hybrid-MIP approaches [30–32]. In this study, 3-ampy-RGO and AgNPs, as well-organized nanocomposites, were used for aptamer immobilization. Firstly, we aimed at coating 3-ampy-RGO on the GCE from without. Afterwards, we had the coating of the AgNPs on the electrode which was modified with 3-ampy-RGO, then, the amine-group of the 3-ampy-RGO was attached to the AgNPs. The resulted combination can be regarded as a suitable platform to attach aptamer-MIP nanohybrid receptor onto the electrode surface. This study aims at combining the advantages of the 3-ampy-RGO with that of AgNPs performance on the 3-ampy-RGO surface. Having in mind the mentioned strategy, the CAP amino-aptamer (NH_2-Apt), with the bonding Ag-N formation, was attached to the AgNPs, as were seen as attachements to the exterior parts of GCE. Besides, it was modified by the 3-ampy-RGO. It is by attaching the aptamer[CAP] complex onto the nanocomposite surface and also the polyresorcinol electropolymerization of this surface that the aptamer[CAP]-MIP nanohybrid was achieved. During the imprinted polymer electrodeposition, the polymer matrix trapped CAP in a way that its molecules would be able to form an interrelation with the resorcinol units. Hydrogen bonding occurs between the NO_2, N—H and O—H groups as being present in CAP, and that of the hydrogen atoms of the O—H groups in the resorcinol units. Accordingly, during the electropolymerization step, we witnessed that it acted as a protective scaffold and also restricted the molecules of the aptamer. In the following step, we washed the modified electrode and, as a result, CAP was removed from the restrained aptamer. In this sense, we achieved a template nanohybrid surface (aptamer-MIP) with CAP rebinding properties. In this sense, we witnessed a change in the electron-transfer quality of $[Fe(CN)_6]^{3-/4-}$, made by the incubation of CAP molecule as the target. It is worth mentioning that one of the most significant advantages of the mentioned system is its ability to detect CAP at 1.0 pM concentration. As far as we know, aptamer-MIP nanohybrid application for targeting the detection of CAP has not been yet reported.

2. Experimental section

2.1. Materials

Chloramphenicol ($C_{11}H_{12}C_{l2}N_2O_5$), silver nitrate ($AgNO_3$), sodium citrate ($Na_3C_6H_5O_7{\cdot}2H_2O$), sodium borohydride ($NaBH_4$), Sodium hydroxide (NaOH) and 3-(aminomethyl)pyridine ($C_6H_8N_2$) were purchased from Sigma-Aldrich Co. LLC (USA). For preparing the phosphate buffered solutions we used 0.1 M Na_2HPO_4 and NaH_2PO_4 and, then, the solutions with different concentrations were prepared by being dissolved in phosphate buffer solution (pH 7.4). Then, we dissolved them in the distilled water in order to obtain DNA solutions. $K_3Fe(CN)_6$, $K_4Fe(CN)_6$, and all other analytical grade reagents were also purchased from Merck or Fluka and, then, used without further purification. For our assays and solutions, we used deionized water. Moreover, throughout our experiments, a solution which contained 5 mM K3Fe(CN)6/K4Fe(CN)6 at a ratio of 1:1 and 0.1 M KCl was applied. All experiments were carried out at room temperature 25 ± 0.5 °C.

The sequence of oligonucleotide follows:

5′-NH_2-ACTTCAGTGAGTTGTCCCACGGTCGGCGAGTCGGTGGTAG-3′

Was purchased from Bioneer Company (South Korea, http://www.bioneer.com) and, then, the aptamer was dissolved in 0.1 M phosphate buffer solution with pH 7.4 was and kept frozen.

2.2. Apparatus and procedures

We performed Electrochemical Impedance Spectroscopy (EIS), Cyclic Voltammetry (CV) and Differential Pulse Voltammetry (DPV) measurements for which we used μ-AUTOLAB electrochemical system type III and FRA2 board computer which was controlled by Potentiostat/Galvanostat (Eco-Chemio, Switzerland) and driven with NOVA software. It is worth noting that a modified GCE was applied as our working electrode, a Pt wire as the counter-electrode and Ag/AgCl electrode as the reference. The DPV measurements were executed in 0.1 M KCl solution which contained 5 mM $K_3Fe(CN)_6/K_4Fe(CN)_6$ with 50 ms pulse period, 25 mV step height, 0.5 s pulse width and 9 mV potential steps. Moreover, within the frequency range of 0.1–10 kHz with 5 mV amplitude, we witnessed the recorded EIS measurements.

The powder X-ray diffraction (XRD) patterns were obtained by a Bruker AXS (D8, Avance) instrument employing the reflection Bragg-Brentano geometry with CuKα radiation. FT-IR spectra were taken with a Jasco FT/IR-680 plus spectrometer. Raman spectra were recorded from 4250 cm^{-1} to 100 cm^{-1} on a high resolution dispersive Raman Thermonicolet (LabRAM HR UV/Vis/NIR, Electrooptics). Transmission electron microscopy (TEM) images were taken with a Philips CM-10 microscope operated at 100 kV. The 3-ampy-RGO nanohybrid was prepared using reported method [33].

2.3. Preparation of actual sample

In order to prepare milk samples, 1 mL of the samples, in 5 mL phosphate buffer solution, was spiked with the suitable CAP concentrations.

2.4. Synthesis of 3-ampy-RGO

It was from flake graphite that Graphene oxide (GO) was prepared applying a modified Hummers method [34–36]. Dispersing (0.01 g) of GO in 100 mL distilled water led to the GO exfoliation by sonication for 10 min. Consequently, a mixture which contained 3-(aminomethyl) pyridine (3-ampy) (0.01 mmol) and 0.01 g NaOH, in distilled water, was then added to the final mixture and subsequently refluxed for 24 h at 80 °C. Finally, there were the black solids that were isolated, washed with distilled water and ethanol and, then, air-dried at room temperature. Besides, 1 mg of 3-ampy-RGO was dispersed to 1 ml of the distilled water for 1 h and was used in the electrode modification step. The synthesis of 3-ampy-RGO are illustrated in Scheme 1.

2.5. Preparation of silver nanoparticles

In accordance to the literature, AgNPs were synthesized [37]. In this method, 24 mL of 100 mM trisodium citrate, l mL of 100 mM silver nitrate aqueous solution, and l mL of 25 mM $NaBH_4$ (which was freshly prepared) were respectively added dropwise to 400 mL of boiled water which had been cooled while stirring. After the reaction was completed under vigorous stirring for 2 h, a transparent, yellow, and homogenous-colloidal solution of AgNPs was reached without any other precipitate. The prepared solution of AgNPs was kept without light for 24 h before use. Besides, UV–Vis spectroscopy and TEM were used for the characterization of the as-synthesized AgNPs.

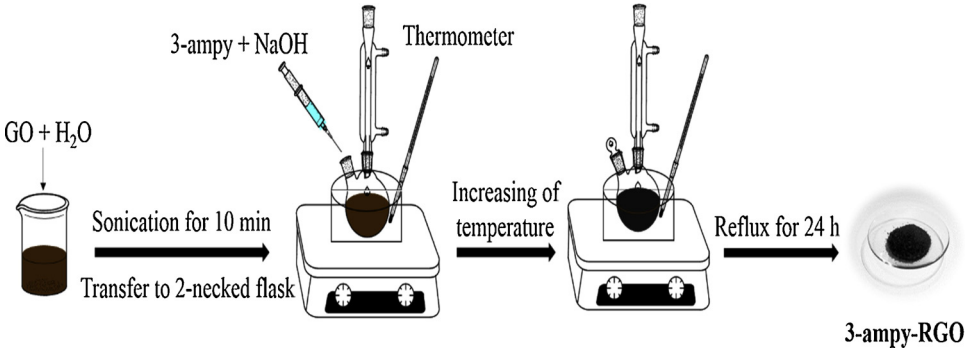

Scheme 1. Schematic illustration of the process of as-synthesizing 3-ampy-RGO.

2.6. The preparation of GCE modified with 3-ampy-RGO and silver nanoparticle

Firstly, the GCE was polished with alumina powder on polishing cloth. Then, in order to remove the adsorbed particles, it was sonicated for 10 min in an ethanol/water (1:1) ultrasonic bath. After drying, 10 μL of 3-ampy-RGO solution was used to cover the GCE surface and, then, it was dried at room temperature in order to form a homogeneous layer. 10 μL of the AgNPs solution was applied to cover the 3-ampy-RGO /GCE for 4 h, then, the amine groups of 3-ampy-RGO were attached to the AgNPs with an Ag-N bonding formation. For the following steps, the prepared electrode was kept for future uses and, also, the resultant platform was denoted as AgNP/3-ampy-RGO /GCE.

2.7. Aptamer-MIP nanohybrid preparation

In continuation of our study, we incubated 30 μL of 10 μM of the aminoaptamer in phosphate buffer solution (pH = 7.4) was incubated with 30 μL of 10 μM of CAP at 37 °C (1 h). Then, onto the surface of the AgNP/3-ampy-RGO/GCE, 10 μL of the resulting aptamer[CAP] complex was dropped for overnight with the purpose of becoming immobilized on the surface. Before performing the molecular imprinting step and in order to saturate any free aminoaptamers on the surface of the aptamer [CAP] complex formation, we applied a drop of 10 μL of 10 μM of CAP to incubate the aptamer[CAP] complex/AgNP/3-ampy-RGO /GCE for 35 min. Then, ultrapure water was used to rinse the electrode as it was dried under N_2 gas. Afterwards, the MIP step was performed using resorcinol monomer polymerization. In this sense, electropolymerization conditions were applied to the 10 mM phosphate buffer solution (pH 7.4) containing 5 mM resorcinol and then electropolymerised using CV (14 cycles, 0–1.2 V vs. Ag/AgCl, scan rate of 100 mV s^{-1}).

Finally, distilled water was used to wash the conditioned electrode and, then, it was stirred overnight in 10 mL of the polar washing solution which contained phosphate buffer solution (2 mL), acetic acid (2 mL), ethanol (4 mL), and acetonitrile (2 mL) at the optimized volume ratio of 2:2:4:2. We used 2 mg of sodium dodecyl sulfate (SDS) for removing the CAP molecules from the surface of the electrode. Because of the CAP polar molecular structure, it is very significant to use the washing solution in order to delete the CAP. Afterwards, we used the distillated water to wash the electrode with the aim of removing the physically weak adsorbed substrates, detergent and remaining solvents. It is worth noting that in the absence of the temple a NIP 'control' electrode (Apt-NIP) was similarly prepared. The synthesis of aptamer-MIP nanohybrid are illustrated in Scheme 2.

3. Results and discussion

3.1. Characterization of the synthesized 3-ampy-RGO

The preparation process of the 3-ampy-RGO is summarized in Fig. S1. FT-IR spectra of GO and 3-ampy-RGO have been illustrated in Fig. 1(1). The FT-IR spectrum of GO which illustrate the peaks at 1054, 1226, 1729 and 3407 cm^{-1} indicate that GO was successfully made [34–36] (Fig. 1(1a)). Besides, Fig. 1(1b) illustrates the 3-ampy-RGO FT-IR spectrum. The peaks at 2865 and 2927 cm^{-1} show vibrations of symmetric νs CH_2 and asymmetric as CH_2 of the 3-ampy, respectively. In this sense, the appearance of the bands at ca. 1575 cm^{-1} (NH) and ca. 1199 cm^{-1} (C—N) gives us more evidences for the 3-ampy presence. Due to the fact that the GO sheet contains reactive groups of epoxy, its exposure to amine groups would bring about a ring opening reaction of the reactive three-membered epoxide ring, constructing C—N and —OH new functional groups. Raman spectroscopy which would be very effective to probe structural and electronic characteristics of graphene materials provides practical information on the defects (D peak) and in plane vibration of sp^2 carbon atoms (G peak) [38]. Fig. 1(2) illustrates the results from Raman spectra of GO and 3-ampy-RGO. The prominent D peak appears from the structural imperfections which have been constructed by attaching epoxide and hydroxyl groups on the carbon basal plane [39]. Moreover, as compared to the G-band position in GO, which is centered at 1583 cm^{-1}, the 3-ampy-RGO G-band shifts to 1598 cm^{-1} (Fig. 1(2)). The G peak blue shift which exists at about 15 cm^{-1} for the 3-ampy-GO corresponds to a possible interaction of 3-ampy molecules and the GO. It would also indicate a better exfoliation of graphene layers [40]. The intensity ratios of ID/IG for GO and 3-ampy-RGO are 0.95 and 1.45, respectively, implying that the size of the sp^2 domains upon localized chemical reduction of the GO by 3-ampy would decrease. The changes in the structure can be studied using XRD patterns. Fig. 1(3) illustrates powder XRD results of graphite, GO and 3-ampy-RGO. Fig. 1(3a) illustrated graphite which showed a very strong 002 peak at 26.3° [41]. While a small change in the principal reflection position was witnessed with oxidation, it was for GO that the most striking difference was the broadness and intensity of the observed peak at 2θ˜10° which corresponded to the (002) plane of the GO illustrated in Fig. 1 (3b) [35]. As it is clear from the Fig. 1(3c), a part of the peak shifted back to the original 002 peak at 25.55° specifically after being functionalized with 3-ampy.

In order to investigate the morphology of the as-synthesized 3-ampy-RGO, TEM analysis has been employed. Fig. 2 illustrates TEM images of GO and 3-ampy-RGO. After the reaction of GO functionalization with 3-ampy, the TEM spectrum of 3-ampy-RGO exhibited more bends and wrinkles as compared to that of the GO nanosheets implying the decreased size of the sp^2 domains under the localized chemical reduction of GO by 3-ampy [42].

3.2. Characterization of the synthesized AgNPs

We examined the spherical AgNPs morphology with TEM image (Fig. S2A). The size range from 8 nm to about 14 nm was observed for NPs diameter. Besides, it is worth mentioning that the UV–Vis spectrum of the ready AgNPs was recorded in the range of 200–500 nm as

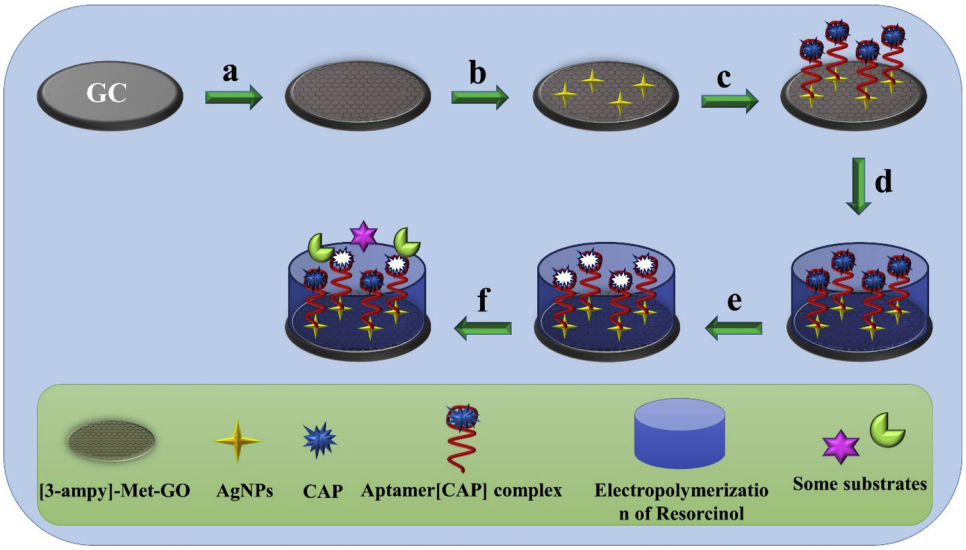

Scheme 2. The schematic diagram of the preparation of the aptamer-MIP nanohybride for CAP detection. (A) Covering of 3-ampy-RGO on the GCE surface; (B) immobilization of the AgNPs on the 3-ampy-RGO/GCE; (C) covalent attachment of aptamer[CAP] complex on the AgNP/3-ampy-RGO/GCE surface; (D) electropolymerization of resorcinol on the aptamer [CAP] complex/AgNP/3-ampy-RGO/GCE; (E) washing the modified electrode with washing solution and removal of the CAP; (F) adding CAP as a target and some antibiotic as interferents.

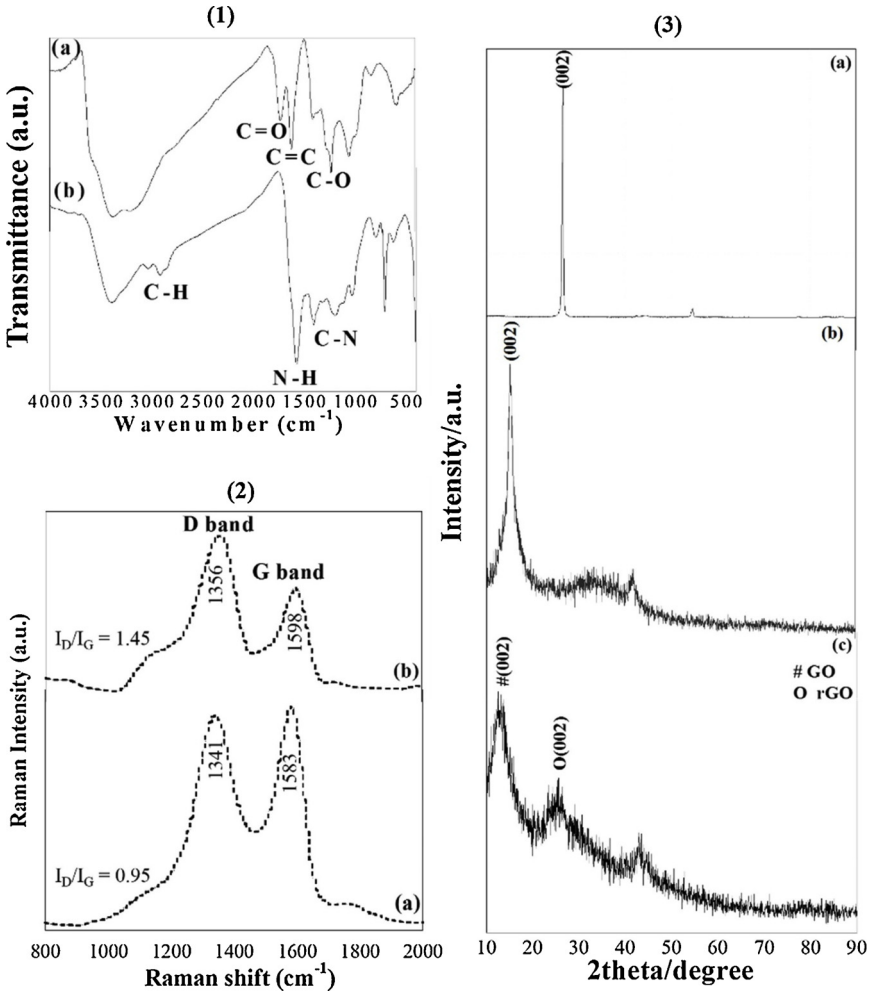

Fig. 1. (1) FT-IR spectra of (1a) GO and (1b) 3-ampy-RGO. (2) Raman spectra of (2a) GO and (2b) 3-ampy-RGO. (3) XRD patterns of (3a) graphite, (3b) GO and (3c) 3-ampy-RGO.

illustrated in Fig. S2B. In accordance to what has been stated before, the observed absorption peak at 398 nm approved the effective synthesis of AgNPs.

3.3. Electrochemical characterization of the stepwise modification process

To probe the successful modification, we applied CV technique. Fig. 3A illustrates the related CV curves in the steps and and also in a solution which contains 5 mM $[Fe(CN)_6]^{3-/4-}$ at a ratio of 1:1 and

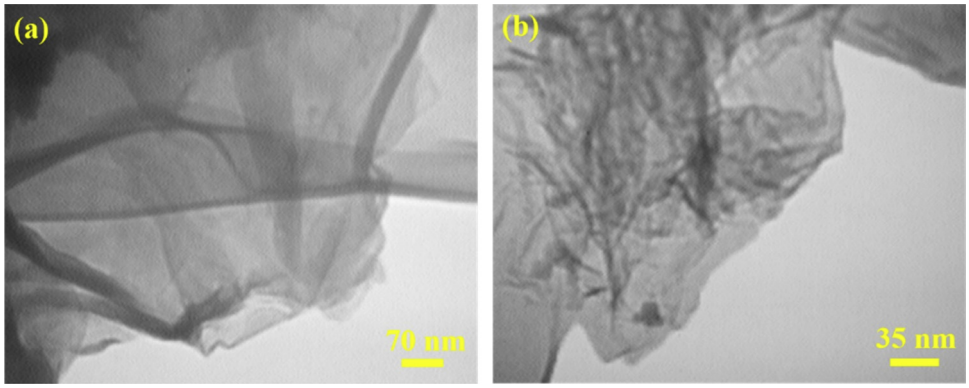

Fig. 2. TEM images of (a) GO and (b) 3-ampy-RGO.

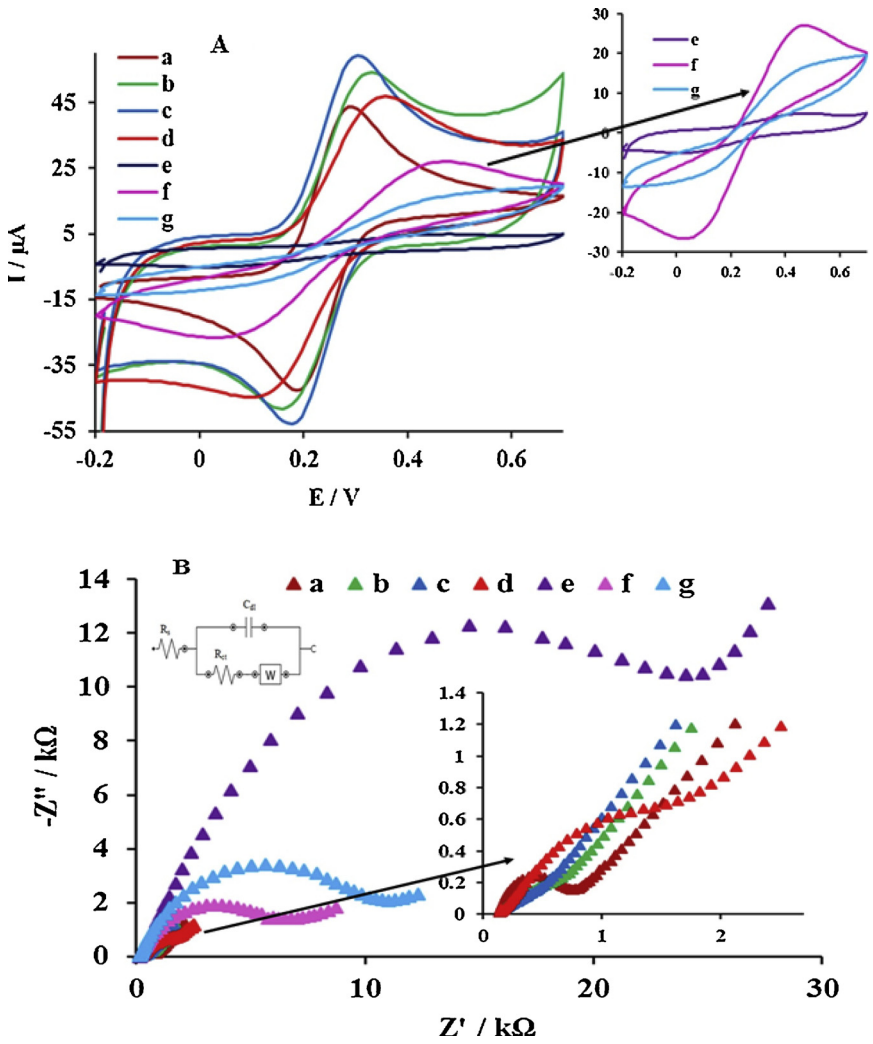

Fig. 3. (a) CVs curve for each steps of modified Electrode, inset is magnification of the last three steps and (b) EIS plots for the Different step of modified Electrode, inset are magnification of the first four steps and the equivalent circuit.

0.5 mM KCl as a redox probe. Fig.3A and B show the bare GCE (a) 3-ampy-RGO/GCE(b), AgNP/3-ampy-RGO/GCE (c), aptamer[CPA]/AgNP/3-ampy-RGO/GCE (d), resorcinol/aptamer[CPA]/AgNP/3-ampy-RGO/GCE (e), aptamer-MIP/AgNP/3-ampy-RGO/GCE (f) and the incubation of CPA(g). Moreover, as it is evident in Fig. 3A, a pair of reversible redox peaks can be perceived at the bare GCE proposing an electrochemical process which is reversible (a). When the 3-ampy-RGO, as a sub-layer, became immobilized on the surface of GCE, we witnessed an increase in the peak current (b). Additionally, the curve b manifested a couple of better-defined redox peaks as compared to that of the bare electrode. Thus, it pointed out the layer of 3-ampy-RGO as exclusive platform, in accordance to the ability of the higher electron transfer, and the active surface area which could significantly increase the present signal.

While the AgNPs were dropped onto the 3-ampy-RGO /GCE surface, the Ag atoms formed a chelate by their interaction with the amine

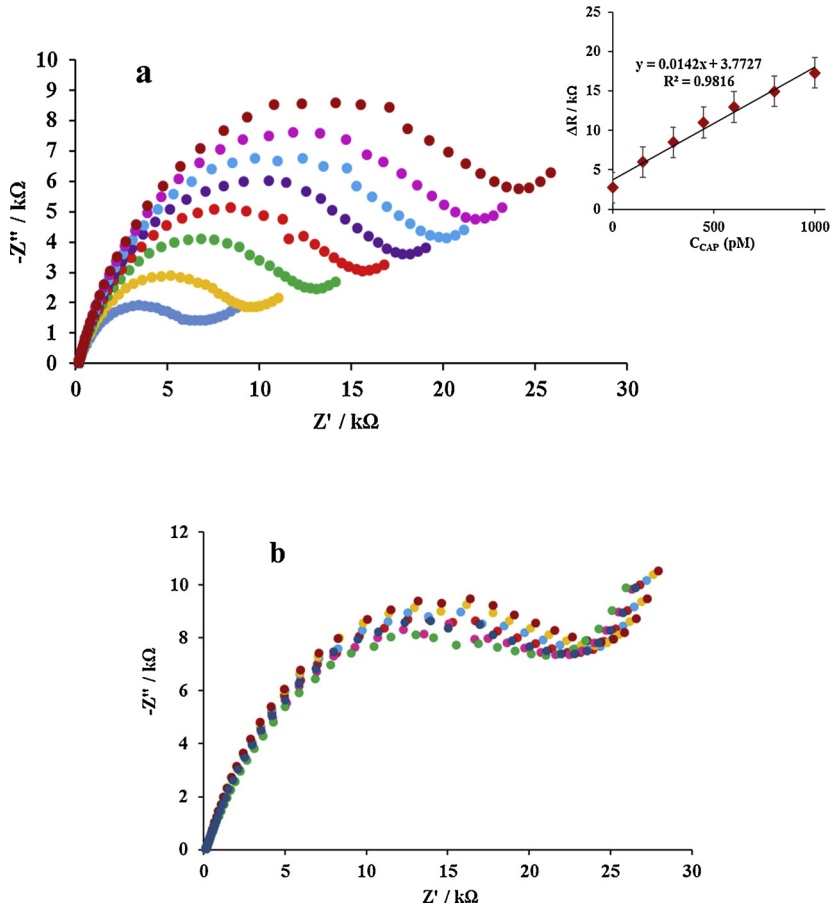

Fig. 4. (a) EIS plots of the aptamer-MIP (b) and aptamer-NIP then incubating with different concentrations of CAP such as 0, 1.0, 150, 300, 450, 600, 800 and 1000 pM. The inset is the plots of the impedimetric response related to aptamer-MIP against of different concentrations of CAP.

groups and the Ag-N bonding formation. Consequently, it resulted in a positive partial charge of amine groups on the 3-ampy-RGO nanomaterial. Thus, the increased peak current was attributed to reduce the repelling between the redox probe anions and 3-ampy-RGO positive partial charge. As a result, the phenomena caused increasing the electron transfer between redox probe and that of the electrode surface (c). This nanocomposite layer would suggest that the AgNP/3-ampy-RGO/GCE is able to accelerate the electron transfer and also to increase the electrode surface area.

As it has been clarified, the peak current of the d curve is lower than that of the CAP, ascribing the attachment of electrodeposited AgNP/3-ampy-RGO/GCE to aptamer[CAP] complex. After the mentioned attachment was done, an obvious decrease of the peak current was witnessed. In this sense, it implies that the aptamer would hinder the electron transfer. When we did the resorcinol electropolymerization on the surface of the aptamer[CAP]/AgNP/3-ampy-RGO/GCE aiming to form MIP cavities, we observed an important decrease in the peak current (e). After washing the imprinted electrode, we witnessed a little increase in peak current (f). It is significant to note that when the resorcinol/aptamer[CPA]/AgNP/3-ampy-RGO/GCE surface is washed with that of the polar washing solution, CAP molecule is generated from the aptamer-MIP fence and, consequently, a better electron transfer is witnessed. Hence, in the aptamer MIP/AgNP/3-ampy-RGO/GCE, the peak current which was lower than that of the aptamer[CAP]/AgNP/3-ampy-RGO/GCE indicated that the polymer remained on the surface after being washed. This small peak current increase showed that both of the CPA removal and also the loss the related resorcinol polymer resulted in the decrease of the steric/conformational restrictions between the redox probe and the surface of the modified electrode [34,43]. By incubating the CAP onto the aptamer-MIP nanohybrid surface and as the sizes of the CAP molecule and the MIP cavity are exactly the same, CAP molecule can match with this space. Thus, we witnessed an increase in the conformational restriction and a decrease in the peak current related to the redox probe (g). The results indicated that aptamer-MIP nanohybrid was successfully prepared.

Next proof for checking the effective synthesized aptamer-MIP nanohybrid was EIS technique. In this regard, two points must be put into consideration: 1) During each modification step, EIS was carried out to characterize the interface of the GCE 2) In order to fix the experimental data, Randles equivalent circuit [R_s (Cdl [R_{ct}W])] was carried out. As it has been clarified from the inset of Fig. 3B, where R_{ct} is the electron-transfer resistance, R_S is considered as the solution resistance, Cdl is the double layer capacitance and Zw is the Warburg impedance. We observed changes in the R_{ct} values upon the stepwise modification of the electrode. When one compares the curves which are related to GCE and 3-ampy-RGO/GCE (a, R_{ct} = 0.750 kΩ, and b, R_{ct} = 0.605 kΩ), a lesser electron-transfer resistance was reached at the 3-ampy-RGO/GCE. After AgNP immobilized on the 3-ampy-RGO/GCE surface, a smaller resistance was witnessed (c) pointing out to the good AgNP/3-ampy-RGO/GCE conductivity (R_{ct} = 0.450 kΩ). The aptamer[CAP] complex was added onto the AgNP/3-ampy-RGO/GCE surface which caused the R_{ct} to become significantly increased (d, 1.45 kΩ) signifying the fact that the electron transfer became more difficult. This value of the R_{ct} indicated that a successful immobilization of the complex of CAP and aptamer was achieved on the surface of the nanocomposite with that of the AgNP in the nanocomposite and amine groups. Afterwards, the attachment of the resorcinol layer in electropolymerization step caused an increase in the R_{ct} value (e, R_{ct} = 24.8 kΩ). This refers to the fact that the electron exchange was significantly blocked between the modified electrode and the redox probe. Then, washing the modified

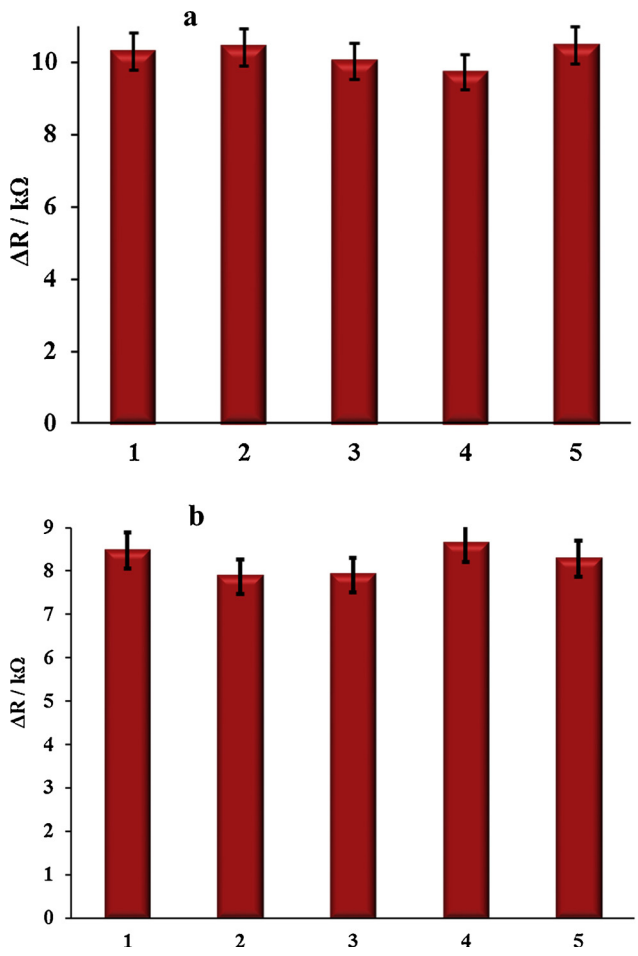

Fig. 5. The ΔR response of the 5 electrodes which modified under the same conditions.

electrode surface and removing the CAP caused a decrease in the steric/conformational restriction. This clarified the fact that electron transfer between the aptamer-MIP nanohybrid surface and that of the redox probe was increased (f, R_{ct} = 6.50 kΩ). CAP incubation on the prepared aptamer-MIP nanohybrid surface hindered the electron transfer and, accordingly, the R_{ct} value was increased to 11.03 kΩ (g). The reaction between CAP and cavity of the aptamer-MIP nanohybrid indicated two specific points: 1) the aptamer molecule captured the CAP 2) in the nanohybrid cavity, we saw the formation of the aptamer[CAP] complex. Here, in this study, the reported EIS data confirmed the results which were obtained by CV disclosing the fact that the sensing interface was successfully achieved.

The electroactive surface area of the sensing platform was calculated by using following Randles Sevcik equation and performing CV at different scan rates [44]:

$$I_p = (2.69 \times 10^5) n^{3/2} A D^{1/2} C^* v^{1/2}$$

In this equation; I_p, n, D ($cm^2\ s^{-1}$), A (cm^2), C*(mol cm^{-3}) and v (Vs^{-1}) denote the peak current of probe, electron transfer number, diffusion coefficient, electroactive surface area, concentration 1.0 mM of $K_4Fe(CN)_6$ + 0.1 M KCl and scan rate of potential sweep, respectively. From the slope of I_p vs $v^{1/2}$ plot the electroactive surface area value of the AgNP/3-ampy-RGO/GCE and GCE was calculated to be 0.32 and 0.06 cm^2, respectively. These results showed a significant improvement in surface area, after modification with AgNP/3-ampy-RGO nanocomposite.

3.4. Analytical application of the CAP aptasensor

In order to probe the method's analytical performance of the, the analytical parameters i. e. the detection limit (LOD) and the concentration linear range were assessed for aptamer-MIP or aptamer-NIP. Analyzing the R_{ct} value of the modified electrode under the CAP presence caused the realization of the CAP detection. Under optimal conditions, the aptamer-MIP or aptamer-NIP have been incubated by various concentrations of CAP for almost 35 min. As it is clear from the Fig. 4a, the amount of R_{ct} is at a minimum amount in the CAP loss, and, consequently, it is progressively increased when the CAP concentration is increased. The ΔR_{ct} was linearly increased with the increase of the CAP concentration in the range of 1.0 pM to 1.0 nM and as R^2 = 0.9816. The regression equation was attained as ΔR_{ct} (Ω) = 0.0142 [CAP] (pM) + 3.7727.

Moreover, based on S/N = 3, a LOD of 0.3 pM was reached. Yet, considering the aptamer-NIP and by the incubation of CAP different concentrations, no important response was witnessed (Fig. 4b). This is because of the aptamer-NIP/GCE possess CAP molecules inside of the

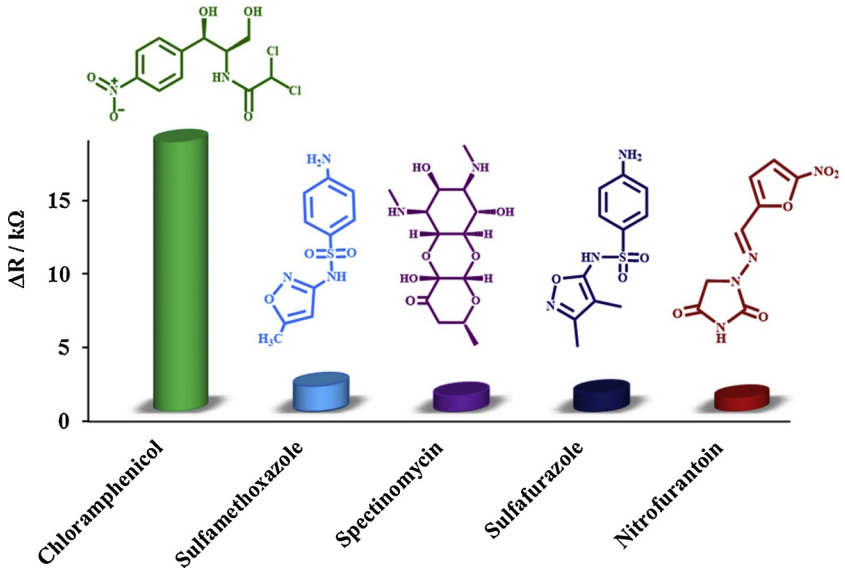

Fig. 6. Bar chart of the ΔR response of the sensor after incubation with CAP (1.0 nM) and interferences such as sulfamethoxazole, spectinomycin, sulfafurazole and nitrofurantoin (100 nM).

Table 1
Detection of chloramphenicol in milk samples.

Samples	Added (nM)	Found by sensor (nM)	Recovery% (n = 3)	Found by fluorescence aptasensing (nM)	Recovery%
Milk 1	0.1	0.105 (± 0.04)	105	0.9 (± 0.01)	90
	1.0	0.98 (± 0.04)	98	1.03 (± 0.02)	103
Milk 2	0.1	0.96 (± 0.03)	96	0.09 (± 0.02)	90
	1.0	1.03 (± 0.04)	103	0.97 (± 0.11)	97

synthetic MIP cavities. Moreover, by the addition of the CAP on this surface and also there existed a lack of the empty cavities on the surface of the modified electrode, the CAP molecules could not bind with aptamer molecules. Consequently, aptamer[CAP] complex won't be formed on the surface of the aptamer-NIP/GCE and, also, with increasing the CAP concentration, the semicircular diameter shows no gradual increase. A comparison of performance of the proposed sensor with some other methods are summered in Table S1. From Table S1, it was found that the linear range and sensitivity of the aptamer-MIP nanohybrid are similar or better than the newly reported methods.

3.5. Optimization of experimental conditions

Providing a sensor with the best performance forced us to optimize the pH value of the solution and, also, the incubation time as our highly important parameters for a high electrochemical response. Due to the fact that the Apt is a biological molecular, the chemical environment must be in such a way not to destroy the Apt. Therefore, there exists an urgent need for a neutral environment. Thus, the experiments were done in a phosphate buffer solution with pH of 7.4. Additionally, the incubation time was examined and it was revealed that the DPV peak current intensity decreased as the incubation time increased from 10 to 70 min, and, more importantly, it reached the minimum value at 35 min. In this sense, 35 min was Selected as the optimal incubation time (Fig. S3).

3.6. Stability, reproducibility, repeatability and selectivity of the method

We evaluated the stability of the mentioned aptasensor. In addition, the response of the fabricated sensor was reported to be 89% of the starting activity after it was kept in refrigerator at 4 °C for 7 days. Besides, we tested the reproducibility of the aptasensor with 5 electrodes. The results can be reproduced according to the fact that the RSD calculation was about 4.3% (Fig. 5a). The repeatability was evaluated by using the same electrode for 5 repeated analyzes. The RSD of the measurements was determined to be 3.8%. These results indicated that the reproducibility and repeatability of the proposed sensor was highly acceptable (Fig. 5b). In order to estimate the method's high selectivity, different interferences, i. e. sulfamethoxazole, spectinomycin, sulfafurazole and nitrofurantoin, are challenged. Fig. 6 illustrates that all of the interferences which created much lower signal, as compared to that of the CAP, demonstrated the excellent selectivity. Performing CVs in the presence of 600.0 pM CAP was used to evaluate the aptamer-MIP nanohybrid stability on the surface of the nanocomposites. The results explained that the peak separation remained unchanged and just 4.8% of the reduction in the peak current happened after at almost 50 repetitive cycles. Finally, it indicated the high stability of the modified electrode (Fig. S4).

3.7. Application of the sensor in actual sample analysis

For the purpose of demonstrating the applicability of the developed sensor, specific amounts of CAP in milk samples were spiked and, then, tested by the recovery method. The results from aptamer-MIP were compared with the results obtained from fluorescence aptasensing analysis using the same samples. Table 1 which illustrates the results confirms that this assay is capable of evaluating the CAP in the actual samples.

4. Conclusion

This study introduced a hybrid probe of aptamer-MIP/AgNP/3-ampy-RGO/GCE in order to construct an easily performed and highly sensitive sensing system for the detection of CAP. The 3-ampy-RGO was applied in order to modify the GCE. AgNPs were immobilized on the NH groups of 3-ampy-RGO via Ag-N bonding formation. Aptamer[CAP] was loaded on the surface of the electrode via the interaction between AgNPs and -NH_2 group of the aptamer. Afterwards, resorcinol electropolymerization around the aptamer[CAP] complexes were applied to enclose the complex as we used molecularly imprinting techniques which were aptasensing and imprinting the recognition safeguard, respectively. After the CAP removal, we witnessed the formation of the double recognition imprinting cavities clarifying the fact that the recognition properties were greater than that of the aptamer. Finally, the sensor's analytical usefulness was demonstrated by analyzing the actual samples. The sensor manifested high selectivity and sensitivity for the detection of CAP because of its dual recognition, and it is also a potential strategy for drug detection.

Declaration of Competing Interest

The authors declare that they have no known competing financial interests or personal relationships that could have appeared to influence the work reported in this paper.

Acknowledgment

This study has been supported by the Department of Chemistry, Faculty of Sciences, Ilam University, Ilam, P. O. BOX. 69315-516, Iran.

Appendix A. Supplementary data

Supplementary material related to this article can be found, in the online version, at doi:https://doi.org/10.1016/j.colsurfb.2019.110451.

References

[1] A. Wang, L. Zhang, Y. Fang, Determination and separation of chloramphenicol and its hydrolysate in eye-drops by capillary zone electrophoresis with amperometric detection, Anal. Chim. Acta 394 (1999) 309–316.
[2] A.A.M. Stolker, U.A.T. Brinkman, Analytical strategies for residue analysis of veterinary drugs and growth-promoting agents in food-producing animals-a review, J. Chromatogr. A 1067 (2005) 15–53.
[3] L. Wang, Y. Zhang, X. Gao, Z. Duan, S. Wang, Determination of chloramphenicol residues in milk by enzyme-linked immunosorbent assay: improvement by biotin – streptavidin-amplified system, J. Agric. Food Chem. 58 (2010) 3265–3270.
[4] J.C. Hanekamp, A. Bast, Antibiotics exposure and health risks: chloramphenicol, Environ. Toxicol. Pharmacol. 39 (2015) 213–220.
[5] L. Yan, C. Luo, W. Cheng, W. Mao, D. Zhang, S. Ding, A simple and sensitive electrochemical aptasensor for determination of chloramphenicol in honey based on target-induced strand release, J. Electroanal. Chem. Lausanne (Lausanne) 687 (2012) 89–94.
[6] M. Gaugain, M.-P. Chotard, D. Hurtaud-Pessel, E. Verdon, Comprehensive validation of a liquid chromatography–tandem mass spectrometry method for the confirmation of chloramphenicol in urine including stability of the glucuronide conjugate and efficiency of deconjugation, J. Chromatogr. B. 1011 (2016) 145–150.

[7] X. Xie, B. Wang, M. Pang, X. Zhao, K. Xie, Y. Zhang, R. Wang, H. Shi, G. Zhang, T. Zhang, Quantitative analysis of chloramphenicol, thiamphenicol, florfenicol and florfenicol amine in eggs via liquid chromatography-electrospray ionization tandem mass spectrometry, Food Chem. 269 (2018) 542–548.
[8] T. Yao, S. Yao, Magnetic ionic liquid aqueous two-phase system coupled with high performance liquid chromatography: a rapid approach for determination of chloramphenicol in water environment, J. Chromatogr. A 1481 (2017) 12–22.
[9] T. Wang, D. Zhang, Z. Zhang, J. Han, Y. Wang, X. Tang, Synchronized separation, concentration and determination of trace chloramphenicol, thiamphenicol and florfenicol in food by using polyoxyethylene cetyl ether-salt aqueous two-phase system coupled with high-performance liquid chromatography, J. Iran. Chem. Soc. 13 (2016) 1759–1765.
[10] W. Huang, H. Zhang, G. Lai, S. Liu, B. Li, A. Yu, Sensitive and rapid aptasensing of chloramphenicol by colorimetric signal transduction with a DNAzyme-functionalized gold nanoprobe, Food Chem. 270 (2019) 287–292.
[11] Y. Xie, Y. Huang, D. Tang, H. Cui, H. Cao, A competitive colorimetric chloramphenicol assay based on the non-cross-linking deaggregation of gold nanoparticles coated with a polyadenine-modified aptamer, Microchim. Acta. 185 (2018) 534.
[12] T.Y. Tan, C. Basheer, K.M. Low, H.K. Lee, Electro membrane extraction of organic acids in undiluted honey with ion chromatographic analysis, Microchem. J. 143 (2018) 234–242.
[13] P. Wu, C. Cai, D. Yang, Y. Zhang, Z. Hu, T. Wang, Determination of three kinds of banned drugs in milk powder by hybrid solid-phase extraction purification combined with gas chromatography and mass spectrometry, J. Sep. Sci. 38 (2015) 3288–3294.
[14] A.R. Cardoso, A.C. Marques, L. Santos, A.F. Carvalho, F.M. Costa, R. Martins, M.G.F. Sales, E. Fortunato, Molecularly-imprinted chloramphenicol sensor with laser-induced graphene electrodes, Biosens. Bioelectron. 124 (2019) 167–175.
[15] A. Munawar, M.A. Tahir, A. Shaheen, P.A. Lieberzeit, W.S. Khan, S.Z. Bajwa, Investigating nanohybrid material based on 3D CNTs@ Cu nanoparticle composite and imprinted polymer for highly selective detection of chloramphenicol, J. Hazard. Mater. 342 (2018) 96–106.
[16] Z. Li, C. Lei, N. Wang, X. Jiang, Y. Zeng, Z. Fu, L. Zou, L. He, S. Liu, X. Ao, Preparation of magnetic molecularly imprinted polymers with double functional monomers for the extraction and detection of chloramphenicol in food, J. Chromatogr. B. 1100 (2018) 113–121.
[17] X. Liang, X. Fang, M. Yao, Y. Yang, J. Li, H. Liu, L. Wang, Direct competitive chemiluminescence immunoassays based on gold@coated magnetic particles for detection of chloramphenicol, Luminescence. 31 (2016) 168–172.
[18] Y. Zhou, C. Sui, H. Yin, Y. Wang, M. Wang, S. Ai, Tungsten disulfide (WS 2) nanosheet-based photoelectrochemical aptasensing of chloramphenicol, Microchim. Acta. 185 (2018) 453.
[19] X. Dang, H. Zhao, X. Wang, T. Sailijiang, S. Chen, X. Quan, Photoelectrochemical aptasensor for sulfadimethoxine using gC 3 N 4 quantum dots modified with reduced graphene oxide, Microchim. Acta. 185 (2018) 345.
[20] Y.-B. Miao, H.-X. Ren, N. Gan, Y. Zhou, Y. Cao, T. Li, Y. Chen, A homogeneous and "off–on" fluorescence aptamer-based assay for chloramphenicol using vesicle quantum dot-gold colloid composite probes, Anal. Chim. Acta 929 (2016) 49–55.
[21] Y. Miao, N. Gan, T. Li, Y. Cao, F. Hu, Y. Chen, An ultrasensitive fluorescence aptasensor for chloramphenicol based on FRET between quantum dots as donor and the magnetic SiO2@ Au NPs probe as acceptor with exonuclease-assisted target recycling, Sensors Actuators B Chem. 222 (2016) 1066–1072.
[22] S. Pilehvar, T. Dierckx, R. Blust, T. Breugelmans, K. De Wael, An electrochemical impedimetric aptasensing platform for sensitive and selective detection of small molecules such as chloramphenicol, Sensors. 14 (2014) 12059–12069.
[23] S.K. Yadav, B. Agrawal, P. Chandra, R.N. Goyal, In vitro chloramphenicol detection in a Haemophilus influenza model using an aptamer-polymer based electrochemical biosensor, Biosens. Bioelectron. 55 (2014) 337–342.
[24] S. Liu, G. Lai, H. Zhang, A. Yu, Amperometric aptasensing of chloramphenicol at a glassy carbon electrode modified with a nanocomposite consisting of graphene and silver nanoparticles, Microchim. Acta. 184 (2017) 1445–1451.
[25] C. Alexander, H.S. Andersson, L.I. Andersson, R.J. Ansell, N. Kirsch, I.A. Nicholls, J. O'Mahony, M.J. Whitcombe, Molecular imprinting science and technology: a survey of the literature for the years up to and including 2003, J. Mol. Recognit. An Interdiscip. J. 19 (2006) 106–180.
[26] O.S. Ahmad, T.S. Bedwell, C. Esen, A. Garcia-Cruz, S.A. Piletsky, Molecularly imprinted polymers in electrochemical and optical sensors, Trends Biotechnol. (2018).
[27] M. Roushani, Z. Rahmati, Development of electrochemical sensor based on molecularly imprinted copolymer for detection of nitrofurantoin, J. Iran. Chem. Soc. (2019) 1–8.
[28] K. Ghanbari, M. Roushani, A. Azadbakht, Ultra-sensitive aptasensor based on a GQD nanocomposite for detection of hepatitis C virus core antigen, Anal. Biochem. 534 (2017) 64–69.
[29] A. Poma, H. Brahmbhatt, H.M. Pendergraff, J.K. Watts, N.W. Turner, Generation of novel hybrid aptamer–molecularly imprinted polymeric nanoparticles, Adv. Mater. 27 (2015) 750–758.
[30] K. Ghanbari, M. Roushani, A nanohybrid probe based on double recognition of an aptamer MIP grafted onto a MWCNTs-Chit nanocomposite for sensing hepatitis C virus core antigen, Sensors Actuators B Chem. 258 (2018) 1066–1071.
[31] F. Shahdost-fard, M. Roushani, Impedimetric detection of trinitrotoluene by using a glassy carbon electrode modified with a gold nanoparticle@ fullerene composite and an aptamer-imprinted polydopamine, Microchim. Acta. 184 (2017) 3997–4006.
[32] S. Li, C. Liu, G. Yin, Q. Zhang, J. Luo, N. Wu, Aptamer-molecularly imprinted sensor base on electrogenerated chemiluminescence energy transfer for detection of lincomycin, Biosens. Bioelectron. 91 (2017) 687–691.
[33] S.J. Hoseini, H.G. Khozestan, R.H. Fath, Covalent attachment of 3-(aminomethyl) pyridine to graphene oxide: a new stabilizer for the synthesis of a palladium thin film at the oil–water interface as an effective catalyst for the Suzuki–Miyaura reaction, RSC Adv. 5 (2015) 47701–47708.
[34] W.S. Hummers Jr., R.E. Offeman, Preparation of graphitic oxide, J. Am. Chem. Soc. 80 (1958) 1339.
[35] S.J. Hoseini, M. Dehghani, H. Nasrabadi, Thin film formation of Pd/reduced-graphene oxide and Pd nanoparticles at oil–water interface, suitable as effective catalyst for Suzuki–Miyaura reaction in water, Catal. Sci. Technol. 4 (2014) 1078–1083.
[36] R.H. Fath, S.J. Hoseini, Copper (I) complex covalently anchored on graphene oxide as an efficient and recyclable catalyst for Sonogashira reaction, Appl. Organomet. Chem. 32 (2018) e3964.
[37] G.-L. Wang, Y.-M. Dong, X.-Y. Zhu, W.-J. Zhang, C. Wang, H.-J. Jiao, Ultrasensitive and selective colorimetric detection of thiourea using silver nanoprobes, Analyst. 136 (2011) 5256–5260.
[38] D. Lee, M. Choi, C. Ha, Polynorbornene dicarboximide/amine functionalized graphene hybrids for potential oxygen barrier films, J. Polym. Sci. Part A: Polym. Chem. 50 (2012) 1611–1621.
[39] K.N. Kudin, B. Ozbas, H.C. Schniepp, R.K. Prud'Homme, I.A. Aksay, R. Car, Raman spectra of graphite oxide and functionalized graphene sheets, Nano Lett. 8 (2008) 36–41.
[40] G. Kalita, S. Sharma, K. Wakita, M. Umeno, Y. Hayashi, M. Tanemura, A photo-induced charge transfer composite of graphene oxide and ferrocene, Phys. Chem. Chem. Phys. 15 (2013) 1271–1274.
[41] S. Khodabakhshi, B. Karami, K. Eskandari, S.J. Hoseini, A. Rashidi, Graphene oxide nanosheets promoted regioselective and green synthesis of new dicoumarols, RSC Adv. 4 (2014) 17891–17895.
[42] R. Sengupta, M. Bhattacharya, S. Bandyopadhyay, A.K. Bhowmick, A review on the mechanical and electrical properties of graphite and modified graphite reinforced polymer composites, Prog. Polym. Sci. 36 (2011) 638–670.
[43] M.E. Lynge, R. van der Westen, A. Postma, B. Städler, Polydopamine—a nature-inspired polymer coating for biomedical science, Nanoscale. 3 (2011) 4916–4928.
[44] A.J. Bard, L.R. Faulkner, Electrochemical Methods, 2nd ed., Wiley, New York, 2001.